

Tamanani, M., Gian, Y. & Ayoub, A. (2016). Evaluation of code criteria for bridges with unequal pier heights. *Bulletin of Earthquake Engineering*, 14(11), pp. 3151-3174. doi: 10.1007/s10518-016-9941-4



**CITY UNIVERSITY  
LONDON**

[City Research Online](#)

**Original citation:** Tamanani, M., Gian, Y. & Ayoub, A. (2016). Evaluation of code criteria for bridges with unequal pier heights. *Bulletin of Earthquake Engineering*, 14(11), pp. 3151-3174. doi: 10.1007/s10518-016-9941-4

**Permanent City Research Online URL:** <http://openaccess.city.ac.uk/15782/>

### **Copyright & reuse**

City University London has developed City Research Online so that its users may access the research outputs of City University London's staff. Copyright © and Moral Rights for this paper are retained by the individual author(s) and/ or other copyright holders. All material in City Research Online is checked for eligibility for copyright before being made available in the live archive. URLs from City Research Online may be freely distributed and linked to from other web pages.

### **Versions of research**

The version in City Research Online may differ from the final published version. Users are advised to check the Permanent City Research Online URL above for the status of the paper.

### **Enquiries**

If you have any enquiries about any aspect of City Research Online, or if you wish to make contact with the author(s) of this paper, please email the team at [publications@city.ac.uk](mailto:publications@city.ac.uk).

# Evaluation of Code Criteria for Bridges with Unequal Pier Heights

Majid Tamanani<sup>1</sup>; Yen Gian<sup>2</sup>, and Ashraf Ayoub<sup>3</sup>

<sup>1</sup> Research Assistant, Department of Civil Engineering, City University London, London, UK, E-mail: [Majid.Mohammadi-Tamanani.1@city.ac.uk](mailto:Majid.Mohammadi-Tamanani.1@city.ac.uk)

<sup>2</sup> Structural Engineer, Jacobs Engineering, London, UK, E-mail: [Yen.Gian.1@city.ac.uk](mailto:Yen.Gian.1@city.ac.uk)

<sup>3</sup> Royal Academy of Engineering Pell Frischmann Chair, Department of Civil Engineering, City University London, London, UK, E-mail: [Ashraf.Ayoub.1@city.ac.uk](mailto:Ashraf.Ayoub.1@city.ac.uk)

## ABSTRACT

One of the challenges associated with Eurocode 8 and AASHTO-LRFD is predicting the failure of irregular bridges supported by piers of unequal heights. EC8 currently uses “moment demand-to-moment capacity” ratios to somewhat guarantee simultaneous failure of piers on bridges, while AASHTO-LRFD relies on the relative effective stiffness of the piers. These conditions are not entirely valid, in particular for piers with a relative height of 0.5 or less, where a possible combination of flexure and shear failure mode may occur. In this case, the shorter piers often result in brittle shear failure, while the longer piers are most likely to fail due to flexure, creating a combination of different failure modes experienced by the bridge.

To evaluate the adequacy of EC8 design procedures for regular seismic behavior, various irregular bridges are simulated through a non-linear pushover analysis using shear-critical fiber-based beam-column elements. The paper investigates the behavior of irregular monolithic and bearing-type bridges experiencing different failure modes, and proposes different methods for regularizing the bridge performance to balance damage. The ultimate aim is to obtain a simultaneous or near-simultaneous failure of all piers irrespective of the different heights and failure mode experienced.

**Key Words:** Irregular bridge; regular design; pier height; shear failure; fiber beam element

## **Introduction**

Bridges are one of the critical components of any transport infrastructure network, and their serviceability during earthquakes is vital to ensure the safety of society. Clearly, bridges have to be designed in a manner that ensures any damage is controllable, and only occur in the place and time that designers intended. One of the challenges associated with Eurocode 8 is to synchronize the failure of irregular bridges with unequal pier heights. Despite the recognized advantages of codes criteria for regularity of bridges, review of literature on seismic behavior of bridges with unequal pier height reveals that the codes criteria may somehow guarantee simultaneous failure [Guirguis and Mehanny 2012, Wei 2014, Abbasi et al. 2015]. However, this might not be true if the ratio of the shorter to longer pier heights is lower than 0.5. This is one of the challenging areas that this paper seeks to address.

In this paper, a finite element model based on a Timoshenko fiber beam-column element formulation [Mullapudi and Ayoub 2010] is used to conduct the study. In this model, concrete is modelled as an orthotropic material in which the principal directions of total stresses are assumed to coincide with the principal directions of total strains, thus changing the direction continuously during the loading. The concrete constitutive laws are accounted for at the fiber level, and the bi-directional shear mechanism at each concrete fiber is modelled by assuming the strain field of the section as given by the superposition of the classical plane section hypothesis with a uniform distribution over the cross-section for the shear strain field. The model was added to the library of elements of the finite element program FEAPpv [Taylor 2012].

## **Eurocode (EC8)**

EC8 codes criteria for regular and irregular seismic behavior of ductile bridges is more focused on piers moment capacity and demands. Bridges are considered to have regular seismic behavior in the horizontal direction when the following conditions are satisfied [Eurocode 8 2013b]:

$$\rho = \frac{r_{max}}{r_{min}} \leq \rho_0 \quad (1)$$

$$r_i = q \frac{M_{Ed,i}}{M_{Rd,i}} \quad (2)$$

In the above equations; ( $r_i$ ) is the local force reduction value for ductile member  $i$ , therefore  $r_{max}$  and  $r_{min}$  are the ( $r_i$ ) maximum and minimum value,  $q$  is the behaviour factor,  $M_{Ed,i}$  is the maximum value of design moment or moment demand of ductile member ( $i$ ) at the intended plastic hinge location, and  $M_{Rd,i}$  is the maximum value of design flexure resistance at the same location. For a bridge to be considered as regular, the value of  $\rho$  has to be less than  $\rho_0$ , which is the recommended value to prevent high ductility demand on one pier. The recommended value is  $\rho_0 = 2$  [Eurocode 8 2013b].

According to EC8 if the bridge is not satisfying the regularity condition, it shall be considered as an irregular bridge, and should be either designed by using a reduced value of  $q$ :

$$q_r = q \frac{\rho_0}{\rho} \geq 1 \quad (3)$$

or should be designed using the result from non-linear analyses in accordance with EC8.

### **AASHTO-LRFD Code**

The AASHTO-LRFD code relates its regularity condition to the effective stiffness, while in EC8 it relates its regularity to the bridge pier flexure strength. AASHTO-LRFD code uses this condition for high seismic zones only. The following condition recommends sets of limited value for ratios between the effective stiffnesses. This effective stiffness is between two columns within a bent or any two bents within a frame [Imbsen, 2006].

The following conditions are for any two bents within a frame or any two columns within a bent, in order to satisfy the condition for regularity to take place [Imbsen 2006]:

$$\frac{K_i^e}{K_j^e} \geq 0.5 \quad (4)$$

$$\frac{K_i^e m_j}{K_j^e m_i} \geq 0.5 \quad (5)$$

In the above equations,  $K_i^e$  and  $K_j^e$  are the smaller and larger effective bent or column stiffness, and  $m_i$  and  $m_j$  are the tributary mass of column or bent.

The following conditions are for adjacent bents within a frame or adjacent columns within a bent:

$$\frac{K_i^e}{K_j^e} \geq 0.75 \quad (6)$$

$$\frac{K_i^e m_j}{K_j^e m_i} \geq 0.75 \quad (7)$$

The previous EC8 and AASHTO-LRFD conditions for regularity of bridges have not been evaluated for bridges with relative height of 0.5 or less, where a combination of flexure and shear failure mode might be present. In this work, the behaviour of irregular bridges for both monolithic and bearing-type cases is evaluated, and code conditions are checked. The description of both types of bridges is presented in the next section. The finite element model adopted is described later.

### **Case Study Bridges**

For the Monolithic-type of connection, two bridge configurations are considered; the first is a three-span bridge with spans 28.0+28.0+28.0m, and the second is a four-span bridge with spans 40.0+50.0+50.0+40.0m. Both bridges are simply supported by two abutments at both ends, which allows for free sliding and rotation about both horizontal axes. Both bridges assume to have a cast-in-place concrete voided slab rigidly connected to the piers. The bridge piers consist of single circular columns with 50mm cover. For both bridges, two different scenarios were considered. For the first bridge, the piers are designed to have the same cross-section with diameter of 1.2 metres. In this case, the first scenario assumes the pier heights ratio to be 0.5 (Fig. 1), and for the second scenario it is 0.35 (Fig. 2). For the second bridge, the piers are designed with the same cross-section with diameter of 2 metres. The first

scenario assumes the bridge to have pier heights of 16 metres, 8 metres and 12 metres (Fig. 3), which makes the pier height ratio between the longer and shorter pier of 0.5, and between the longer and medium pier 0.75. The second scenario assumes the bridge to have pier heights of 16 metres, 6 metres and 12 metres (Fig. 4), with pier height ratio of 0.37 between the longer and shorter pier. Table (1) documents these bridge configurations as case studies I-IV.

For the bearing-type connection, one bridge configuration with three-spans of 28.0+28.0+28.0m is considered. The bridge is supported by two abutments at both ends, and has its deck resting on the piers through fixed pot bearings. The first proposed bearing-type case-study is a bridge with 14.0m and 7.0m pier heights (pier height ratio of 0.5), and the second case study is a bridge with 14.0m and 4.2m pier heights (pier height ratio of 0.3). The piers are circular in shape and sized at 0.6 m diameter initially with one layer of 37 longitudinal bars. The transverse reinforcement initially consists of 32 mm bars, with a spacing of 400 mm. The longitudinal and transverse reinforcements are applied to both piers of the bridge irrespective of their heights. Table (1) documents these bridge configurations as case studies V-VI.

Two additional case study bridges are considered. These are similar to case studies V-VI, except that the connection for the longer pier is assumed to be monolithic, while that for the shorter pier is kept as bearing-type. These mixed-type of connections are referred to as case studies VII-VIII in Table (1).

Finally, case study bridges I and IV are further investigated under the effect of seismic loading through time history dynamic analysis. These cases are noted as case studies IX and X in Table (1).

### **Design for Monolithic and Bearing-type Bridge Piers**

For the structural design of bridge piers, the Oasys-Adsec software is adopted in this research [Oasys 2010]. The software is used to analysis and design column for axial force and moments, and automatically provides a list of acceptable reinforcement arrangements. The Oasys-Adsec software is set to the EN 1992-1-1:2004 EC 2 [Eurocode 2 2004], and the design procedure steps are carried out by specifying the pre-selected diameter of piers and choosing appropriate parameter for slenderness ratio, pier height, axial load and minimum nominal cover. As a result the software automatically calculates all the possible option for reinforcement arrangement, and also generates an axial force-bending moment interaction diagram. The calculation methods used in Oasys-AdSec depend on the assumptions made in material models, and in this case it has been chosen from the material model that are recommended in EN 1992-1-1 Eurocode 2 (2004).

Response Spectrum Analyses is performed in order to calculate design seismic action imposed on the piers in the software Oasys-AdSec, and determine appropriate reinforcement ratios. In this research study, Type 1 elastic response spectrum is considered from EC8 [Eurocode 8 2013a]. The ground type is C which, according to Table 3.1 in EC8 [Eurocode 8 2013a] is dense sand and gravel, consequently, the soil factor is  $S = 1.15$  and characteristics period are  $T_B = 0.2s$ ,  $T_C = 0.6s$  and  $T_D = 2.5s$ . The location of the bridge is assumed to be in seismic zone of moderate and high seismicity with ground acceleration of  $a_{gR} = 0.16g$ , therefore the structure has high importance factor of  $\gamma_I = 1.0$  and lower bound factor of  $\beta = 0.2$ .

For the purpose of this research, in order to account for inelastic behaviour of the bridge, the behaviour factor ( $q$ ) is used in the calculation of pier reinforcement. The behaviour factor ( $q$ ) is specified in Table 4.1 of EC8 [Eurocode 8 2013a]. It has been chosen for ductile reinforced concrete with  $q=3.5\lambda(as)$ ;  $\lambda(as)$  is taken to be 1.0, therefore the behaviour factor is  $q=3.5$ .

The design spectrum can be derived as shown in Fig. 5 and reduced by the behaviour factor “q”.

### **Finite Element Frame Model of Case Study Bridges**

In this research, the case study bridges are modelled with two-dimensional frame elements as shown in Figs. 6-8. The bridge deck is modelled according to EC8 recommendations which state that “the bridge deck shall remain within the elastic range under seismic loads [Eurocode 8 2013a].” As a result, it is modelled as an elastic isotropic frame element.

The superstructure superimposed load is assumed to equal 190kN/m. Axial loads for the seismic analysis are assumed to be lumped; and according to EC8, the lumped masses include the dead load in addition to 20% of the live loads [Eurocode 8 2013a]. Consequently for the bridge with two piers, the first and second piers are subjected to an axial load of 5320kN (4256kN dead load + 1064kN live load); while in the case study with three piers, the first and third piers are subjected to an axial load of 8550 kN (6840kN dead load + 1710kN live load), while the second pier is subjected to 9500 kN (7600kN dead load + 1900kN live load).

The bridge piers are modelled with one fiber-based Timoshenko beam-column element. The element used follows a force-based approach with exact interpolation of the moment and shear functions [Mullapudi and Ayoub 2010], and therefore only a single element is deemed suitable for the finite element discretization. A brief description of the element is provided in the next section. The pier cross-section is assumed to be circular, with circular reinforcement arrangement and transverse spirals/pitch. In this type of section, the continuous confinement of concrete is provided by the transverse reinforcement, which protects longitudinal bars from buckling. In the model, the cross-section is divided into several fibers along the radial and tangential directions as shown in Fig. 9. Each fiber follows a specific material model, being steel or concrete. The uniaxial concrete constitutive law follows the modified Kent and Park model [Park et al. 1982] and the biaxial rules follow the model described in the next



section; while the steel constitutive law follows the uniaxial Menegotto-Pinto model [Menegotto and Pinto 1973]. Failure of an element is defined when the lateral load carrying capacity is reached.

The material properties used in the finite element model are defined according to EC8 (ANNEX E) for non-linear analyses [Eurocode 8 2013a], and are shown in Table (2).

### **Fibre-based Beam-Column Timoshenko Element**

In order to model bridge piers, a shear-critical fibre-based beam-column element is adopted [Mullapudi and Ayoub 2010]. The advantage of this type of element is that it can predict both bending and shear failure with the use of a single finite element with six degrees of freedom.

In this model, the concrete is assumed to follow an orthotropic constitutive relation in which the directions of orthotropy are the principal directions of total strain. The shear mechanism at each concrete fiber of a cross-section is modeled by assuming the strain field of the section as given by the superposition of the classical plane section hypothesis for the longitudinal strain with a uniform distribution over the cross-section for the shear strain field. Transverse strains are internal variables determined by imposing equilibrium between concrete and transverse steel. Element forces are obtained by performing equilibrium based numerical integration on section axial, flexural, and shear behavior along the length of the element. The values of the concrete equivalent uniaxial strains in principal directions 1-2 have three conditions, and the strength in one direction is affected by the strain state in the other direction. The equivalent uniaxial strains are derived from the biaxial strains with the help of the modified Poisson Ratios of cracked concrete, also called the Hsu/Zhu ratios [Zhu and Hsu 2002]. The three concrete strain conditions are as follow:

The first condition is 1-Tension, 2-Compression: In this case, the equivalent uniaxial concrete strain  $\bar{\varepsilon}_1$  in principal direction 1 is in tension, and strain  $\bar{\varepsilon}_2$  in principal direction 2 is in compression. Due to this condition, the uniaxial concrete stress  $\sigma_1$  in direction 1 is calculated

as a function of  $\bar{\varepsilon}_1$ , while the compressive strength in principal direction 2,  $\sigma_2$  will soften due to the tension in the orthogonal direction. Vecchio (1990), Belarbi and Hsu (1995), and Hsu and Zhu (2001) derived a softening equation in the tension-compression region based on panel testing. The latter equation is used in this model:

$$\zeta = \left( \frac{5.8}{\sqrt{f'_c (MPa)}} \leq 0.9 \right) \left( \frac{1}{\sqrt{1 + 400\bar{\varepsilon}_1}} \right) \left( 1 - \frac{|\alpha_{r1}|}{24^\circ} \right) \quad (8)$$

where  $\zeta$  is the softening coefficient,  $\alpha_{r1}$  is the deviation angle which is the difference between the applied principal stress angle and the rotating crack angle based on strains,  $\bar{\varepsilon}_1$  is the lateral tensile strain, and  $f'_c$  is the peak compressive strength.

The ultimate stress in the orthogonal direction is then calculated as follow (Fig. 10):

$$\sigma_{2p} = \zeta f'_c \quad (9)$$

The second condition is 1-Tension, 2-Tension: The equivalent uniaxial strain of concrete  $\bar{\varepsilon}_1$  in direction 1 is in tension, and the equivalent uniaxial strain  $\bar{\varepsilon}_2$  of concrete in direction 2 is also in tension. In this case, the uniaxial concrete stress in direction 1 is evaluated from  $\bar{\varepsilon}_1$ , and similarly the stress in direction 2 is evaluated from  $\bar{\varepsilon}_2$ .

Finally the third condition is 1-Compression, 2-Compression: both principle directions are in compression. The current research uses the Vecchio's (1992) simplified version of Kupfer et al. (1969) biaxial compression strength equation. The concrete compressive strength increase in one direction depends on the confining stress in the orthogonal direction.

To validate the finite element model, two correlation studies with experimentally tested shear-critical column specimens available in the literature are presented. The first is the rectangular column HC4-8L 16-T6-0.2P tested by Xiao and Martirosyan (1998). The geometry and loading details of the column are given in the reference by these authors. In this

test, shear failure was observed at the column, followed by core degradation. Fig. 11 shows the experimental and analytical load-deformation behavior of the column. The figure confirms the proposed finite element model can properly depict the response. The second specimen is column SC3 tested by Aboutaha et al. (1999). This column had a small amount of transverse reinforcement, which resulted in a shear failure. Fig. 12 shows the experimental and analytical response of the column. Again, the figure confirms the accuracy of the finite element model.

### **Proposed criteria to verify EC8 regularity conditions**

In order to properly evaluate the EC8 regularity criteria, the  $\rho$  factor defined in Equation (1) is first computed for the case study bridges. However, in order to account for deformation demands, a new similar term noted  $\rho_D$  that defines the ratio between maximum and minimum displacements of piers up to the failure point is proposed. The  $\rho_D$  factor is generally better to use to judge the regularity of the bridge. A  $\rho_D$  value of 1 means all piers for a given bridge fail simultaneously, irrespective of the difference between their heights. The  $\rho_D$  factor is computed from nonlinear analysis of the case study bridges using the model described above; then compared to the EC8 term.

### **Investigating EC8 recommendation for case study bridges**

#### **I. Three-span monolithic-type bridge with pier height ratio of 0.5:**

A pushover analysis was performed for this case study with pier height ratio of 0.5. The reinforcement ratio for the short and long piers was 1.7% and 2.63%, respectively. The transverse reinforcement for the initial design was assumed initially to be the same as 16mm diameter and the required spacing for both piers was 100mm. As a result the peak lateral load for the 7m and 14m piers are 1421 kN at 73.2mm and 994 kN at 292mm respectively as shown in Fig.13 and Table 3. Therefore the displacement ratio  $\rho_D = 4$  while, the corresponding value based on EC8 is  $\rho = 1.75$ , which is less than the recommended value of

$\rho = 2$  indicating a regular response. However according to the results from the pushover analysis, it is clear that here the bridge is irregular.

In order to synchronize the failure, the transverse reinforcement of the short pier is decreased to 10mm diameter at 245mm spacing while the transverse reinforcement of the long pier is kept the same as the initial assumption. The modified spacing of the shorter column satisfies the minimum spacing requirements according to EC8. These changes in the shorter pier affected the maximum lateral load and displacement so that they are more closely similar to the longer pier (Fig. 14). The  $\rho_D$  factor in this case reaches 1, indicating simultaneous failure of both piers.

## II. Three-span monolithic-type bridge with pier height ratio 0.35:

Shear-displacement curve from pushover analysis shows unsynchronised failure of bridge piers. In this bridge, the short pier fails at a shear capacity of 1656.4kN and 43mm displacement, while the failure occurs in the long pier at a shear capacity of 996.2kN and 290mm displacement (Fig. 15 and Table 4). Consequently, the displacement ratio between the long and short pier is ( $\rho_D = 6.74$ ), while the corresponding EC8 regularity  $\rho$  factor equals 1.59. It is clear that the flexural strength of the long pier is much greater than the shorter pier. The shorter pier showed signs of a high stiffness and quickly experienced brittle shear failure as expected. The results also show that the longer pier of 14m gives a larger displacement at its maximum load, indicating that the ductility is greater in the longer pier.

In order to synchronize the failure, the transverse reinforcement of the short pier is changed to 10mm diameter at 270mm. In this case, the shear capacity of the short pier is 1232.7kN and displacement is 307.6mm, while the displacement for the long pier at the point of failure of the bridge is 319mm, making the  $\rho_D$  factor equals to 1.04 (Fig. 16). The corresponding EC8 regularity  $\rho$  factor at this point equals 1.25. Noting that this is a small difference from the initial EC8 regularity  $\rho$  factor, it is clear that the EC8  $\rho$  factor remains nearly constant for

varying levels of transverse reinforcement of the short pier. This is due to the fact that EC8 uses “moment demand-to-moment capacity” ratios to guarantee simultaneous failure of piers on bridges, while here the bridge is regularized by change in the shear capacity.

#### III. Four-span monolithic-type bridge with pier height ratio 0.5:

Looking at the shear-displacement curve in Fig. 17 and the values in Table (5), it clearly represents an unsynchronised failure of all piers within the bridge. The shear capacities for the piers with 16 metre, 8 metre and 12 metre heights are 3624.7kN, 4390.4kN and 4077.4kN, respectively. Displacements at the failure points are 307.4mm, 142.7mm and 207.2mm for the piers respectively. For this particular bridge, transverse reinforcement with diameter of 20mm and 100mm spacing are assumed for all three piers. For the purpose of this research the transverse reinforcement was kept constant for the long pier, while gradually decreased for the medium and short piers in order to have synchronised failure for all piers. The value of  $\rho_D$  approaches 1 (Fig. 18) when the transverse reinforcement is 20mm diameter with 205mm spacing for the medium pier and 20mm diameter with 235mm spacing for the short pier. In this case, the shear capacity of the short pier is 3688kN, while the initial shear capacity was 4433kN; therefore, from a strength point of view, there is a 745kN reduction. However, on the other hand, ductility is increased in the short pier and a regular behaviour is observed.

#### IV. Four-span monolithic-type bridge with pier height ratio 0.37:

In this case study, it has been further noted that the optimum value of  $\rho_D \approx 1$  corresponds to a small transverse reinforcement value in the short pier (Figs. 19-20). However, when  $\rho_D \approx 1$ , the shear capacity of the pier reduces to 3816.9kN, the pier became more ductile and displacement increased to 342mm.

From a pushover analysis, it has been noted that for the case study bridges with monolithic connections, the  $\rho$ -factor pre-specified by EC8 suggested that the bridge is regular, while the

corresponding  $\rho_D$  value retrieved from nonlinear analysis to judge the regularity is higher than 1. The gap between the  $\rho_D$  value and  $\rho$  factors even increases as the difference between pier heights increases. In other word, despite the EC8 pre-specified  $\rho$ -factor, it does not guarantee simultaneous failure of bridges with different pier height. As the shear capacity changes in the shorter pier in order to have  $\rho_D \approx 1$ , EC8  $\rho$ -factor stayed nearly constant.

V. Three-span Bearing-type bridge with pier height ratio 0.5:

In this case study bridge, the peak lateral load for the 7 m pier is about 1330 kN and the peak lateral load for the 14 m pier is about 480 kN (Fig. 21). The transverse reinforcement of the 7m pier was changed to 6 mm bars at 400 mm spacing while the longitudinal reinforcement of the 7m pier is adjusted to a layer of 37@24 mm bars. These changes in the shorter pier affected the maximum lateral load and displacement to be more closely similar to the longer pier.

By reducing the longitudinal reinforcement of the shorter pier to allow a smaller transverse reinforcement, the behaviour of the overall structure has become more regular in the sense that both piers fail at a closer point. It is however visible that the shorter pier continues to fail sooner than the longer pier (Fig. 22). It is logical to believe that reducing the size of the transverse reinforcement or increasing the spacing will create a simultaneous failure, but it is not recommended for the transverse reinforcing bars to be reduced to any lower than 6 mm in diameter and the spacing not to exceed 400 mm. Further, the lateral displacement in this case is quite large which can cause off-seating at the abutment, a factor that needs to be checked before the design is finalized.

VI. Three-span Bearing-type bridge with pier height ratio 0.3:

The pier height ratio is reduced to 0.3 with the long and short piers being 14m and 4.2m respectively. The change in height of the shorter pier has significantly affected the overall stiffness of the pier as shown by the steeper slope of the curve (Fig. 23). The reduced length

of the pier resulted in a shear failure that is much anticipated at less than 100 mm displacement. From analysis of the model, it is predicted that a transverse reinforcement of 6 mm or less is needed for the 4.2 m pier to fail simultaneously with the 14 m pier. An attempt to regularize the failure of the piers is shown here, where the transverse reinforcement is reduced to 6 mm, which is the lowest recommended size, and where the longitudinal reinforcement is changed to a layer of 37@24 mm bars to allow the 6 mm transverse bars to be suitable.

However, applying the 6 mm transverse reinforcement bars does not create sufficient ductility for the 4.2 m pier to fail simultaneously with the 14 m pier although an improvement in regularity is observed (Fig. 24).

#### VII. Three-span combination of bearing and monolithic connection bridge with pier height ratio 0.5:

To find another solution that could be used for regularising pier performance of bearing-type bridges, the connection between the pier and superstructure is further investigated. In this case, a combination of monolithic and bearing-type connections for each pier is studied. Using the original geometry and reinforcements of the previous case study bridges highlighted previously, the longer 14 m pier is connected monolithically to the deck. The lateral load experienced by both piers of the bridge becomes very similar, at around 1000 kN. This is a reduction in peak lateral load for the shorter pier, and a significant increase in peak lateral load for the longer pier. The displacement at which the shorter pier fails also increased slightly while the displacement at which the longer pier fails has decreased (Fig. 25). Creating a rigid connection in the 14 m pier therefore decreases its ductility and increases its flexural strength.

The transverse reinforcement for the 7 m pier is then reduced to steel rebars of 8 mm in diameter. The results shown below indicates that the 7 m pier continues to shows shear

behaviour and reaches yielding at around 300 kN but the failure points of both piers are near simultaneous (Fig. 26). Unlike the bridge models previously analysed with bearing connections, the ultimate load of the shorter pier is lower than the 14 m pier due to the high flexural strength of the long pier generated by its rigid connection to the bridge deck. Reducing the transverse reinforcement for the shorter pier reduced the maximum load from about 1000 kN to about 850 kN.

VIII. Three-span combination of bearing and monolithic connection bridge with pier height ratio 0.3:

A reduction in the shorter pier to 4.2 m, as expected, shows an increase in stiffness compared to bridges with height ratio of 0.5 (Fig. 27). After regularization, due to its short length, the maximum force of the short pier is now just above 1000 kN which is very similar to the maximum force of the longer pier (Fig. 28). The maximum displacement for both piers is also similar at roughly 930 mm before failure. Both piers of the bridge show unique behaviour but have similar levels of ductility with these chosen reinforcements. The bridge appears to be regular in design and both piers will fail almost simultaneously.

IX. Three-span monolithic-type bridge with pier height ratio of 0.5 under seismic excitations:

In order to confirm the results obtained from the static analysis conducted earlier, a seismic analysis is conducted for case study bridge # I under the effect of El Centro earthquake record. An Incremental Dynamic Analysis (IDA) (Vamvatsikos and Cornell, 2002) is performed for the irregular bridge by scaling the record up to the failure point. The dynamic load deformation response is shown in Fig. 29, which clearly depicts an irregular behaviour for the two piers. After regularization using the same procedure as for case study bridge # I, the dynamic load deformation behaviour depicts a near simultaneous failure at around -0.33m



as shown in Fig. 30. These results confirm the conclusion derived from the static analysis case.

- X. Four-span monolithic-type bridge with pier height ratio 0.37 under seismic excitations:

Similar to case IX, an Incremental Dynamic Analysis was conducted for the irregular four-span bridge evaluated in case study IV. Fig. 31 shows the long pier fails at a displacement much larger than that of the other two piers. After regularization similar to case study bridge # IV, all piers have a nearly simultaneous failure point as shown in Fig. 32.

### **Section-Fibre Analyses**

In the present research, Section Fibre Analysis was performed for the pier sections, to generate stress-strain curves within the cross-section of the pier for the transverse as well as longitudinal steel bars in the tension zone. The Section Fibre Analyses was performed for the case study bridges in order to verify the results obtained from pushover analyses.

As an example, the results for case study bridge # IV are shown in Figs. 33-34 for the transverse and longitudinal reinforcement respectively. The results clearly show that the transverse steel hasn't reached its yield strength point before regularising the bridge, while the longitudinal bar reached its yield strength with constant strength level. On the other hand, by increasing the spacing (decreasing the confinement), the transverse steel reach the yield strength with higher ductility. The longitudinal bars also attract higher strains. As a conclusion, the results showed that suitable arrangement of the transverse reinforcement will result in increase in ductility of the concrete piers.

### **Conclusion**

The following conclusions can be drawn from the study. These conclusions are limited to piers with relative height ratio of 0.3-0.5, and aspect ratio of 7-26.67:

1. It has been concluded that EC8 conditions for regular bridge design are not entirely valid. Satisfying EC8 design procedures for regular seismic behaviour does not necessarily result in synchronised failure of bridge piers with unequal height, particularly for relative height of 0.5 or less.
2. Bridges with unequal pier height with relative height of 0.5 or less have combinations of flexure and shear failure modes. In this case, the shorter piers often result in brittle shear failure which limits their ductility capacity, while the longer piers are most likely to fail due to flexure. As a conclusion, if the short piers are designed based on flexure, they might have an over-strength that could result in an opposing effect with respect to regularization.
3. Bridges with piers of unequal height with relative height of 0.5 or less could have a synchronised failure by having suitable arrangements of transverse reinforcement. Furthermore, it has been noted that by decreasing the transverse reinforcement ratio, the transverse steel could reach yielding resulting in higher ductility. These conclusions were confirmed through both static and dynamic analyses.
4. Introducing a monolithic connection for the long piers in bearing-type bridges decreases the pier ductility. However, a monolithic connection for the long piers is advantageous as it significantly increases its flexural strength, allowing a more even load distribution and therefore better regular design of the bridge.

## References

- Abbasi, M., Zakeri, B., and Amini, G. G. (2015). Probabilistic Seismic Assessment of Multiframed Concrete Box-Girder Bridges with Unequal-Height Piers, *Journal of Performance of Constructed Facilities*, ASCE, doi: 10.1061/(ASCE)CF.1943-5509.0000753, 2015.
- Aboutaha, R.S., Engelhardt, M.D., Jirsa, J.O., and Kreger, M.E. (1999). Rehabilitation of Shear Critical Concrete Columns by Use of Rectangular Steel Jackets, *ACI Structural Journal*, 96(1): 68-78.
- Belarbi, A. and Hsu, T.T.C. (1995). Constitutive Laws of Softened Concrete in Biaxial Tension-Compression, *ACI Structural Journal*, 92(5): 562-573.
- Eurocode 2 (EC2) (2004). Design of concrete structures general rules and rules for buildings, Ref.No PrEN 1992-1-1.
- Eurocode 8 (EC8), (2003a). Design of Structures for Earthquake Resistance - Part 1: General Rules, Seismic Actions and Rules For Buildings, Ref.No PrEN 1998-1.
- Eurocode 8 (EC8) (2003b). Design of Structures for Earthquake Resistance - Part 2: Bridges”, Ref.No PrEN 1998-2.
- J. E. B. Guirguis and S. S. F. Mehanny (2012). Evaluating code criteria for regular seismic behaviour of continuous concrete box girder bridges with unequal height piers, *Journal of Bridge Engineering*, ASCE, 18(6): 486-498.
- Hsu, T.T.C., and Zhu, R. H. (2001). Softened Membrane Model for Reinforced Concrete Elements in Shear, *ACI Structural Journal*, 99(4): 460-469.
- Imbsen, R. A. (2006). Recommended LRFD guidelines for the seismic design of highway bridges, NCHRP Project 20-07/Task 193, Transportation Research Board, National Research Council, Washington, DC.
- Kupfer, H. B., Hildorf, H. K., and Rusch, H. (1969). Behavior of concrete under biaxial stresses, *ACI Structural Journal*, 66(8): 656–666.
- Menegotto, M., Pinto, P.E. (1973). Method of Analysis for Cyclically Loaded Reinforced Concrete Plane Frames Including Changes in Geometry and Non-Elastic Behavior of Elements Under Combined Normal Force and Bending, *Proceedings, IABSE Symposium on Resistance and Ultimate Deformability of Structures Acted on by Well-Defined Repeated Loads*, Lisbon, pp. 15-22.
- Mullapudi, T.R.S, and Ayoub, A. (2010). Modeling of the seismic behaviour of shear-critical reinforced concrete columns, *Engineering Structures* 32, 3601-3615.
- Park, R, and Priestley, M.J.N, Gill, W.D (1982). Ductility of Square Confined Concrete Columns, *Journal of Structural Engineering*, ASCE, 108(4): 929-950.
- Taylor, R.L. (2012). A finite element analysis program, personal version 3.1 user manual. Oasys ADC Manual (2010), [online] Available: <http://www.oasys-software.com/>
- Vamvatsikos, D., and Cornell, C.A. (2002). Incremental Dynamic Analysis, *Earthquake Engineering and Structural Dynamics*, 31(3): 491-514.
- Vecchio, F.J. (1990). Reinforced concrete membrane element formulation, *Journal of Structural Engineering*, ASCE 116: 3, 730-750.
- Vecchio FJ. (1992). Finite element modeling of concrete expansion and confinement, *Journal of Structural Engineering*, ASCE; 118(9):2390–405.

Wei, S.S. (2014). Effects of Pier Stiffness on the Seismic Response of Continuous Bridges with Irregular Configuration, *Applied Mechanics and Materials*, 638-640: 1794-1802.

Xiao, Y., and Martirosyan, A. (1998). Seismic Performance of High-Strength Concrete Columns, *Journal of Structural Engineering, ASCE*, 124(3): 241-251.

Zhu RH, Hsu TTC. (2002). Poisson effect of reinforced concrete membrane elements, *ACI Structural Journal*, 99(5):631-40.

Table 1: Case Study Bridges

| <i>Case study</i> | <i>Spans</i>         | <i>Connection</i> | <i>No. of pier</i> | <i>Piers</i> | <i>Pier heights ratio</i> | <i>Analysis Type</i> |
|-------------------|----------------------|-------------------|--------------------|--------------|---------------------------|----------------------|
| I                 | 28.0+28.0+28.0m      | Monolithic        | Two                | 14 & 7m      | 0.5                       | Static               |
| II                | 28.0+28.0+28.0m      | Monolithic        | Two                | 14 & 5m      | 0.35                      | Static               |
| III               | 40.0+50.0+50.0+40.0m | Monolithic        | Three              | 16, 8 & 12m  | 0.5                       | Static               |
| IV                | 40.0+50.0+50.0+40.0m | Monolithic        | Three              | 16, 6 & 12m  | 0.37                      | Static               |
| V                 | 28.0+28.0+28.0m      | Bearing           | Two                | 14 & 7m      | 0.5                       | Static               |
| VI                | 28.0+28.0+28.0m      | Bearing           | Two                | 14 & 4.2m    | 0.3                       | Static               |
| VII               | 28.0+28.0+28.0m      | Mixed             | Two                | 14 & 7m      | 0.5                       | Static               |
| VIII              | 28.0+28.0+28.0m      | Mixed             | Two                | 14 & 4.2m    | 0.3                       | Static               |
| IX                | 28.0+28.0+28.0m      | Monolithic        | Two                | 14 & 7m      | 0.5                       | Dynamic              |
| X                 | 40.0+50.0+50.0+40.0m | Monolithic        | Three              | 16, 6 & 12m  | 0.37                      | Dynamic              |

Table 2: Material Properties used in Finite Element Model

| Concrete C30/37 properties              |                         |
|---|-------------------------|
| Compressive strength                    | $f'_c = 30 \text{ MPa}$ |
| Strain at reaching the maximum strength | $\varepsilon_o = 0.003$ |
| Ultimate strain                         | $\varepsilon_u = 0.014$ |
| Steel reinforcement properties          |                         |
| Yield stress                            | $f_y = 420 \text{ MPa}$ |
| Young's modulus                         | $E_s = 200 \text{ GPa}$ |

Table 3: Detail from initial design for the bridge piers with ratio of 0.5

|                            | First Pier. 14m | Second Pier. 7m |
|----------------------------|-----------------|-----------------|
| Maximum Lateral Force (kN) | 994.75          | 1421.7          |
| Maximum Displacement (mm)  | 292.24          | 73.217          |

Table 4: Detail from initial design for the bridge piers with ratio of 0.35

|                            | First Pier. 14m | Second Pier. 5m |
|----------------------------|-----------------|-----------------|
| Maximum Lateral Force (kN) | 996.2           | 1656.4          |
| Maximum Displacement (mm)  | 290.86          | 47.309          |

Table 5: Detail from initial design for the bridge with 16, 8 and 12 metre pier heights

|                            | First Pier.<br>16m | Second Pier.<br>8m | Third Pier.<br>12m |
|----------------------------|--------------------|--------------------|--------------------|
| Maximum Lateral Force (kN) | 3624.7             | 4390.4             | 4077.4             |
| Maximum Displacement (mm)  | 307.42             | 142.75             | 207.25             |

Table 6: Detail from initial design for the bridge with 16, 6 and 12 metre pier heights

|                            | First Pier.<br>16m | Second Pier.<br>6m | Third Pier.<br>12m |
|----------------------------|--------------------|--------------------|--------------------|
| Maximum Lateral Force (kN) | 3625.4             | 4804.6             | 4083.9             |
| Maximum Displacement (mm)  | 300.54             | 112.70             | 209.75             |

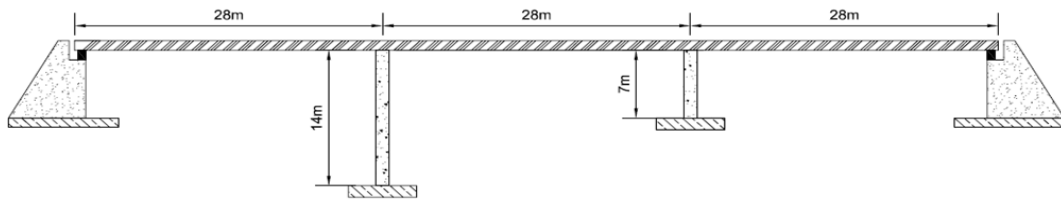


Fig. 1: Bridge arrangement for the first scenario of the bridge with two piers

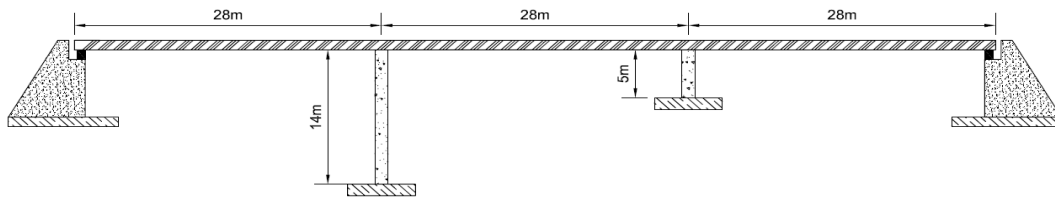


Fig. 2: Bridge arrangement for the second scenario of the bridge with two piers

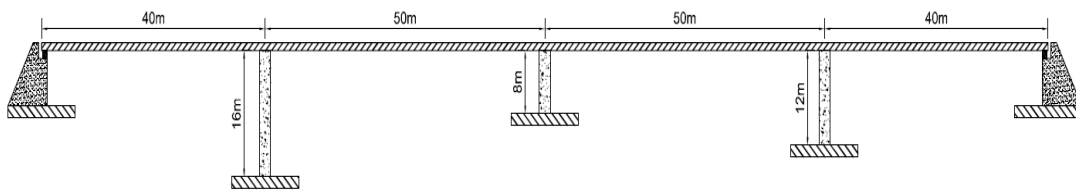


Fig. 3: Bridge arrangement for the first scenario of bridge with three piers

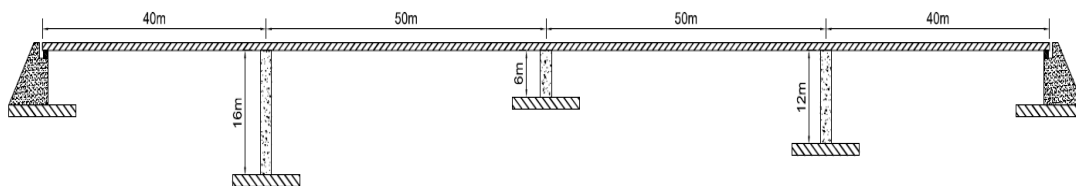


Fig. 4: Bridge arrangement for the second scenario of bridge with three piers



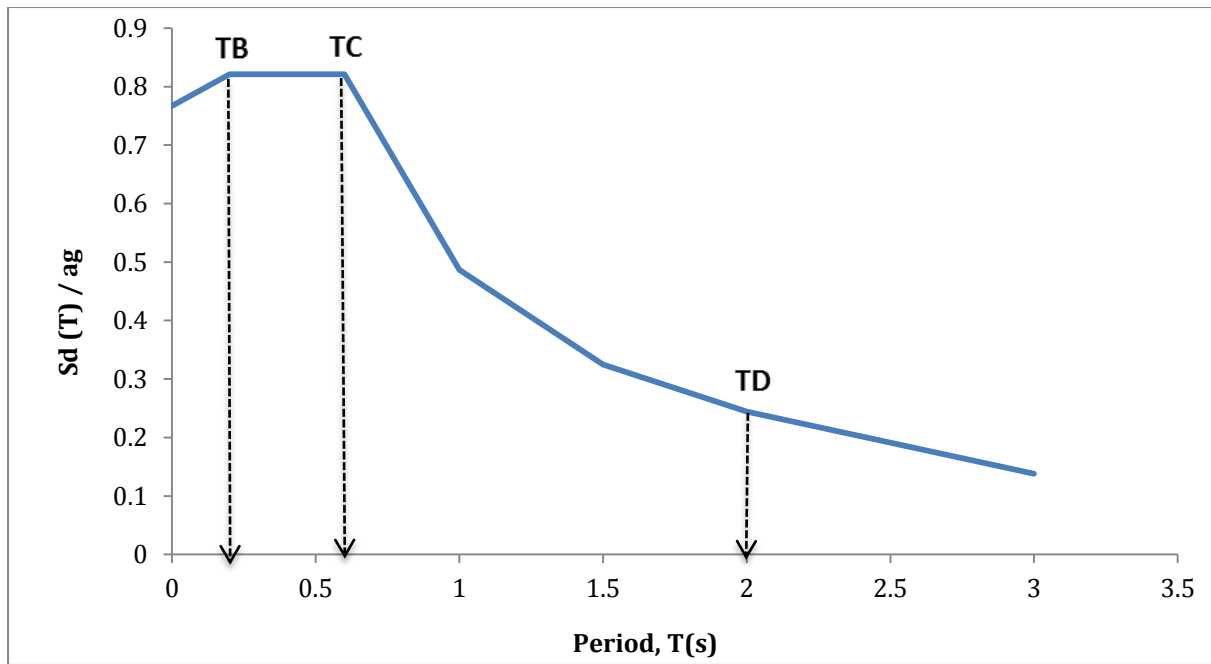


Fig. 5: Design response spectrum for the design of case study bridges

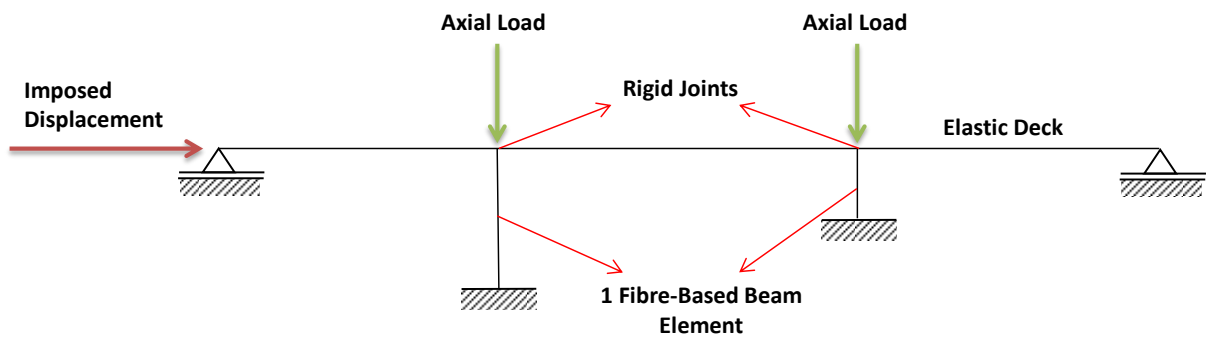


Fig. 6: Modelling using 2D frame elements for bridge with Monolithic type Connection

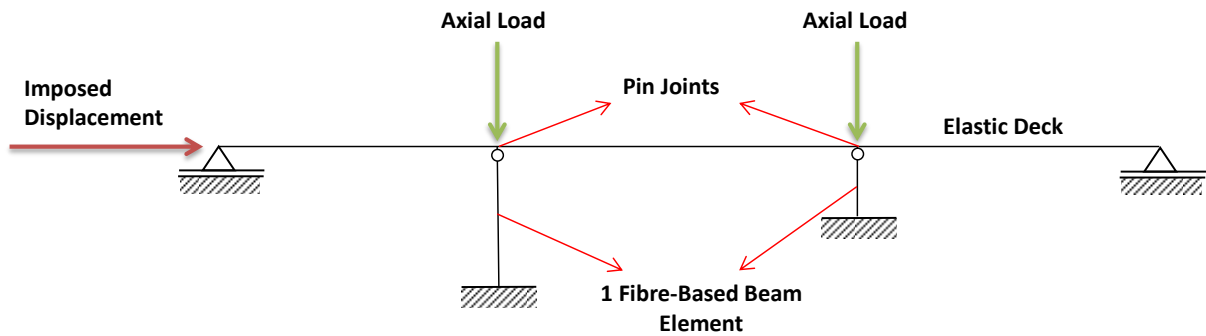


Fig. 7: Modelling using 2D frame elements for bridge with Bearing type Connection

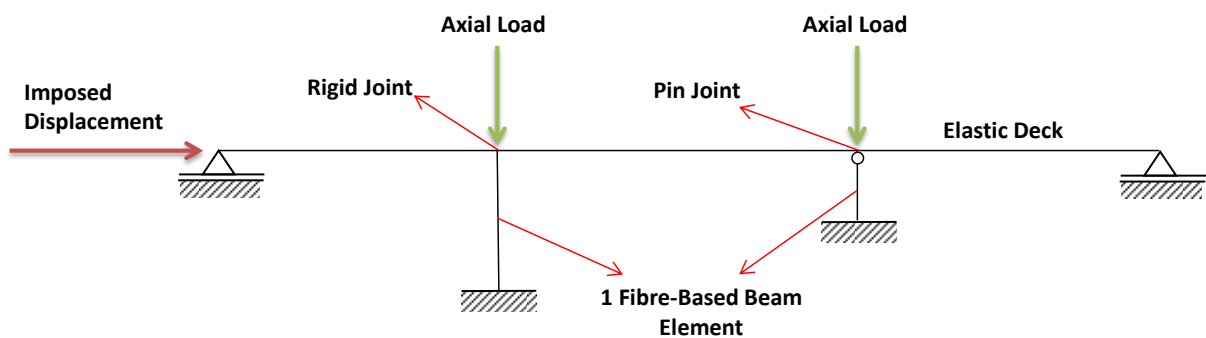


Fig. 8: Modelling using 2D frame elements for bridge with mixed type of connection

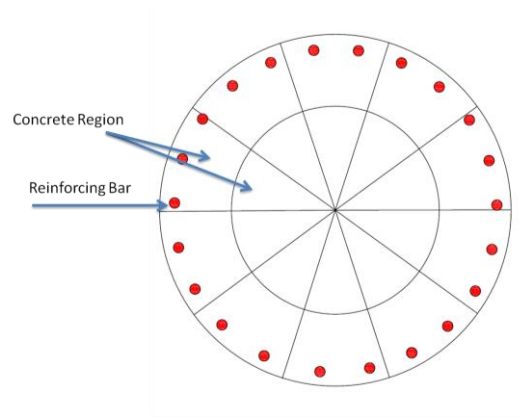


Fig. 9: Sample modelling of pier cross-section for the section-fibre analysis

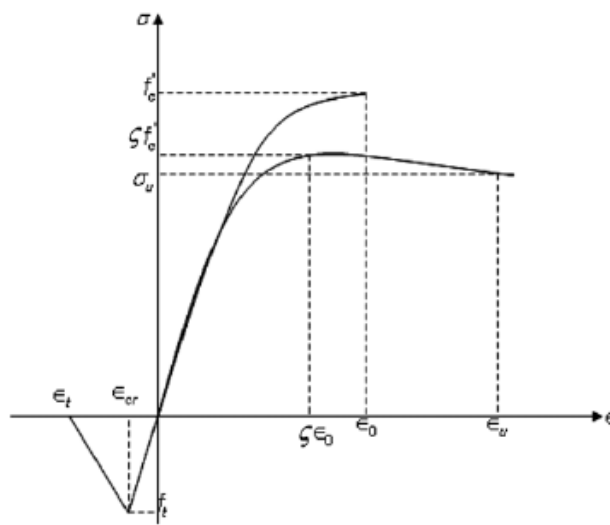


Fig. 10: Stress-strain curve with softening

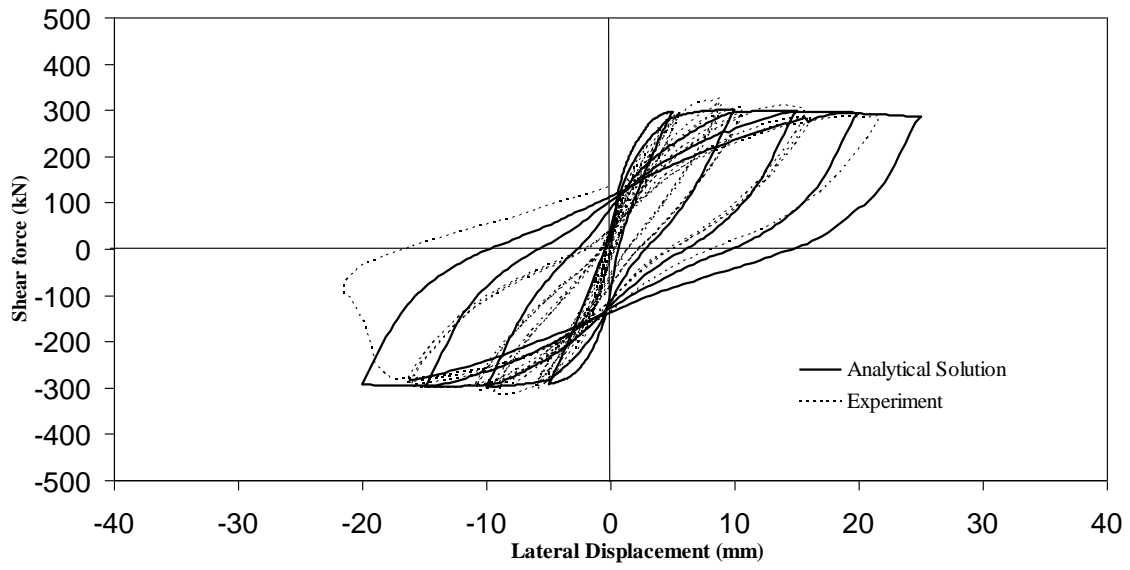


Fig. 11 Behavior of Xiao and Martirosyan (1998) column HC4-8L 16-T6-0.2P

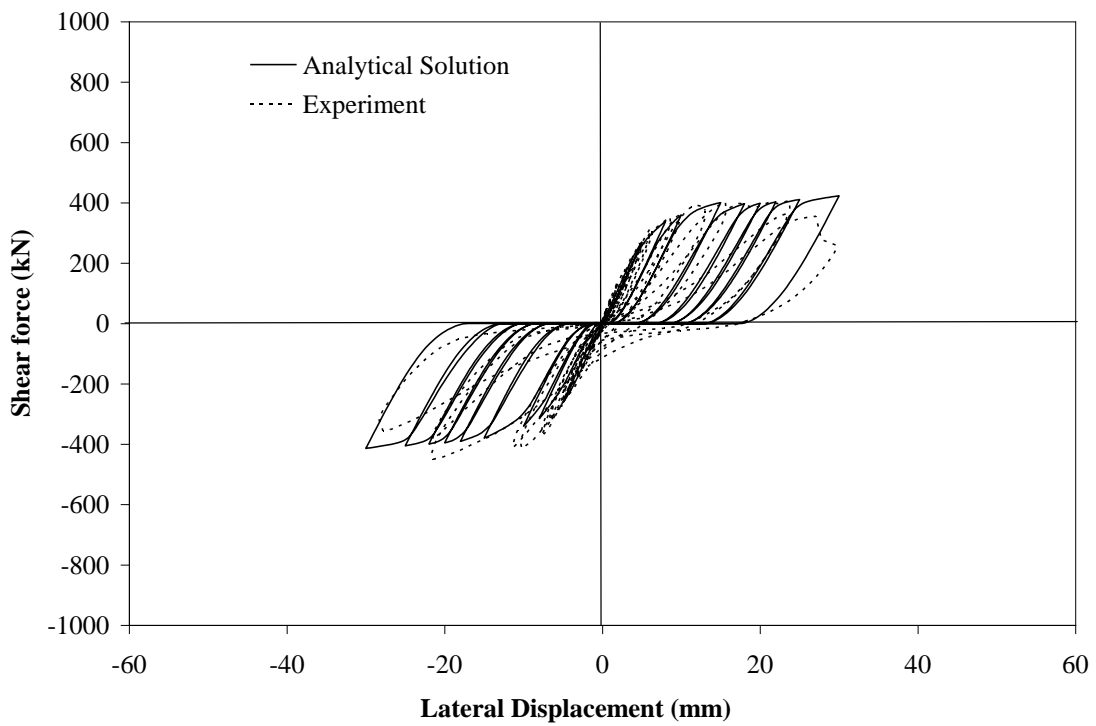


Fig. 12 Behavior of Aboutaha et al. (1999) Column SC3

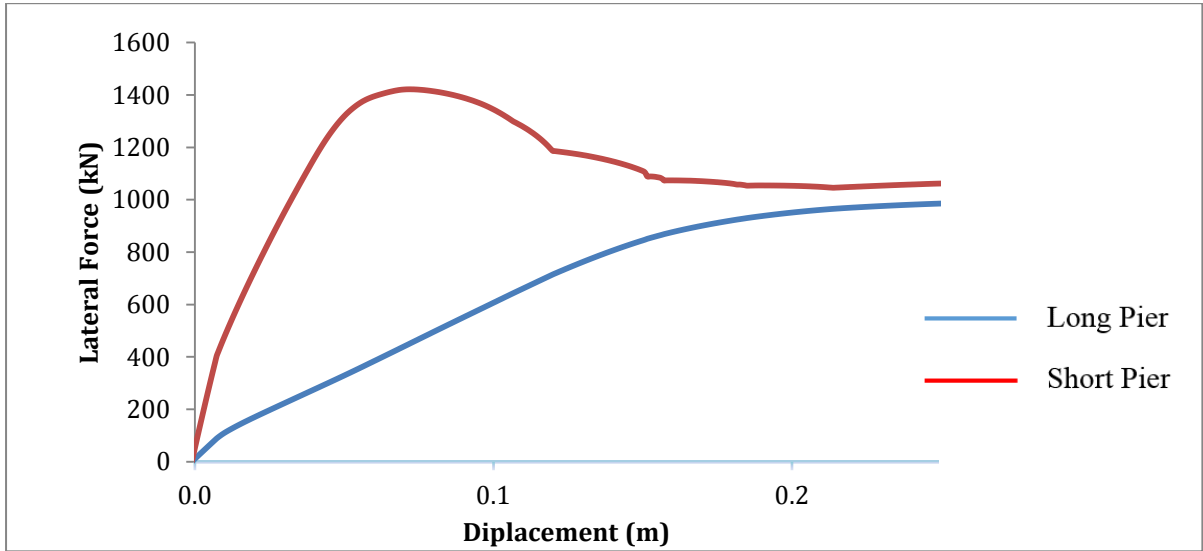


Fig. 13: Shear-displacement curve showing unsynchronised failure of bridge with pier height ratio of 0.5

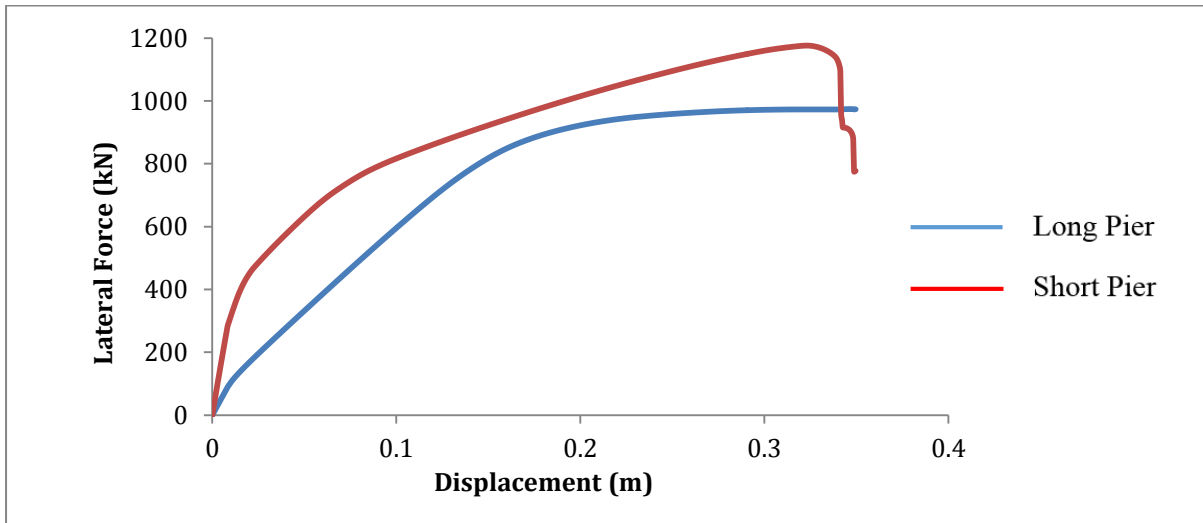


Fig.14: Shear-displacement curve showing synchronised failure of bridge with pier height ratio of 0.5

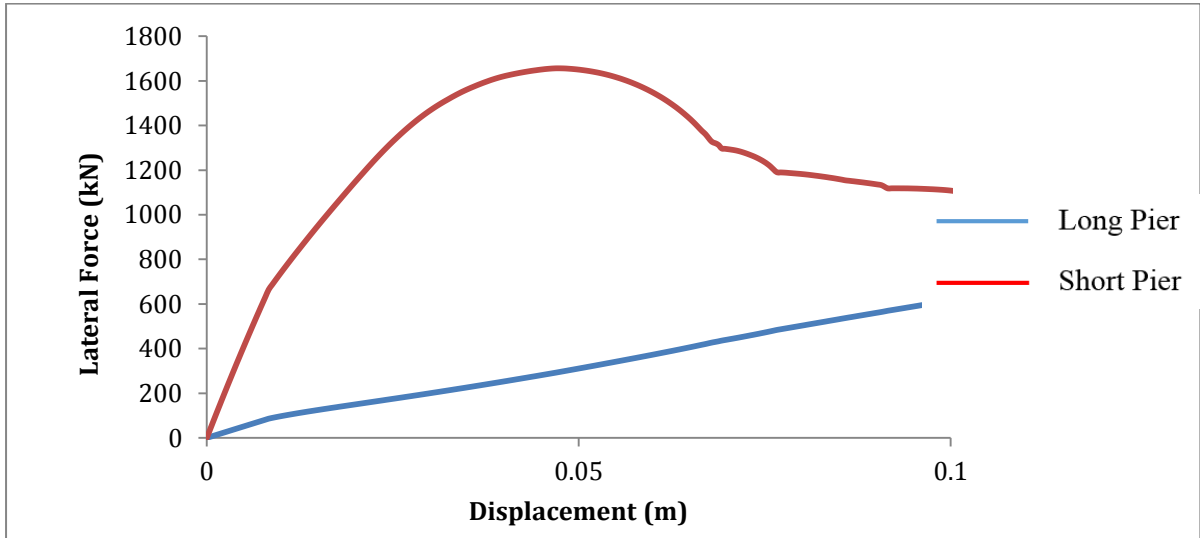


Fig.15: Shear-displacement curve showing unsynchronised failure of bridge with pier height ratio of 0.35

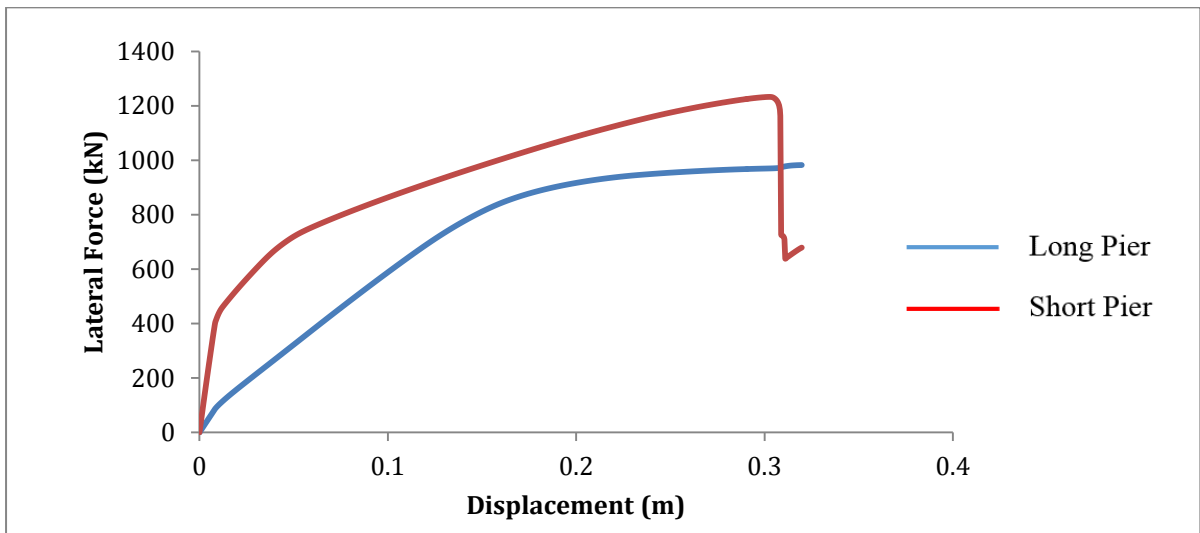


Fig.16: Shear-displacement curve showing synchronised failure of bridge with pier height ratio of 0.35

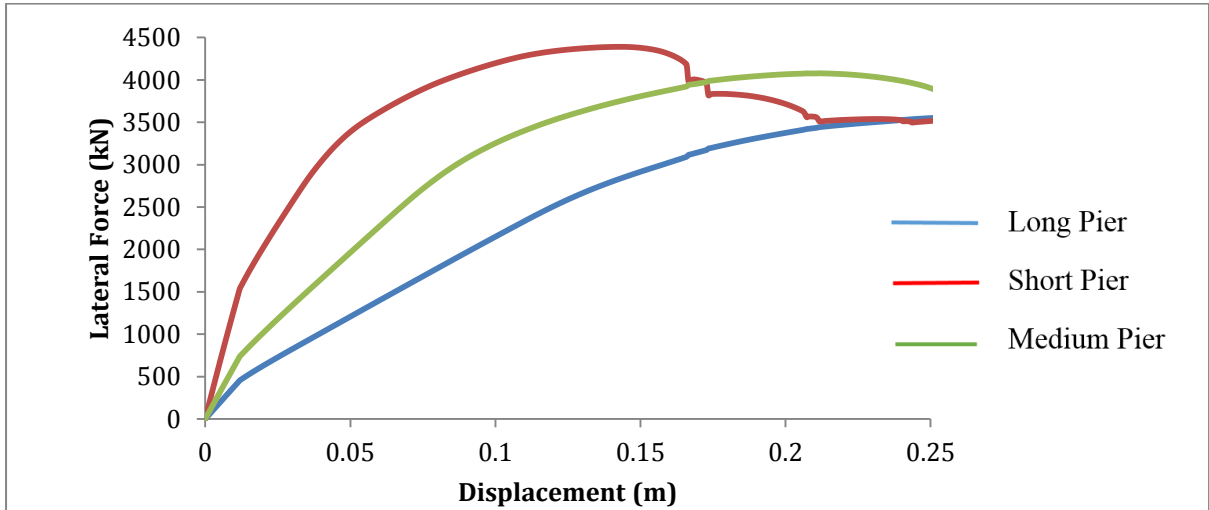


Fig.17: Shear-displacement curve showing unsynchronised failure of bridge with 16, 8 and 12 metre pier heights

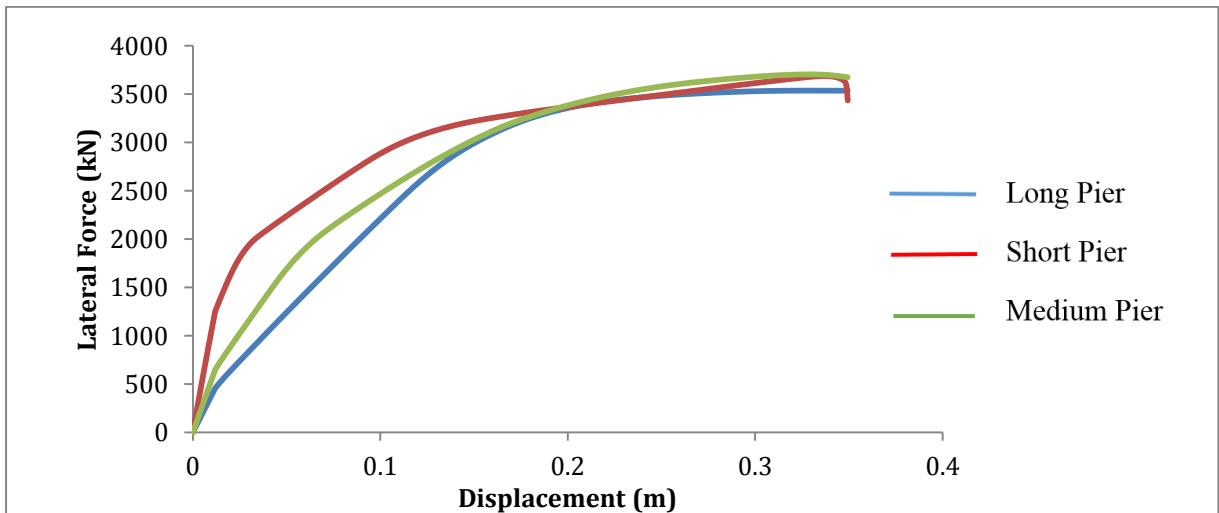


Fig.18: Shear-displacement curve showing synchronised failure of all piers with from first scenario of the second case study

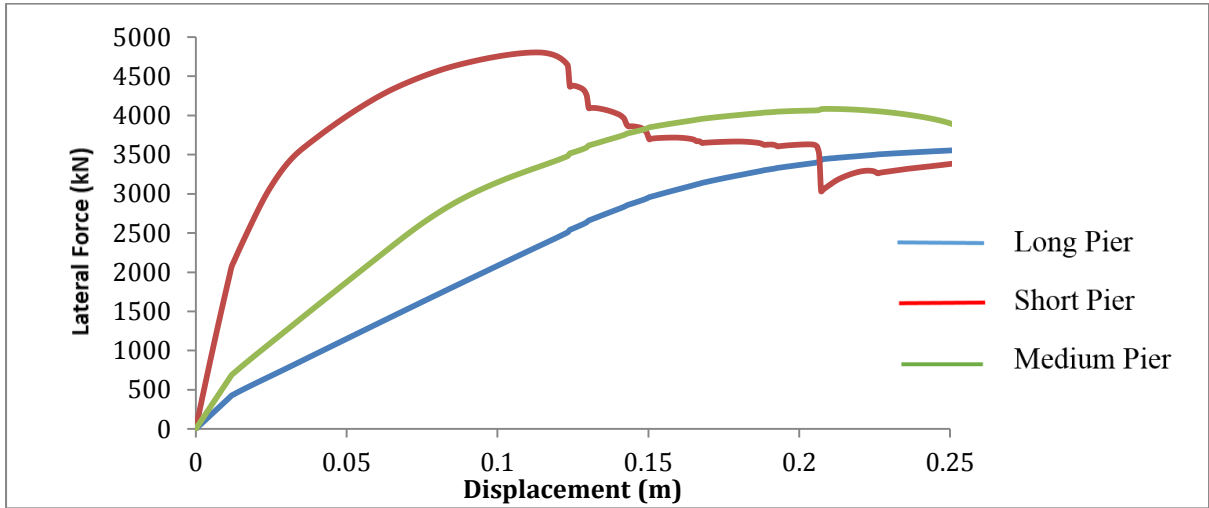


Fig.19: Shear-displacement curve showing unsynchronised failure of bridge with 16, 6 and 12 metre pier heights

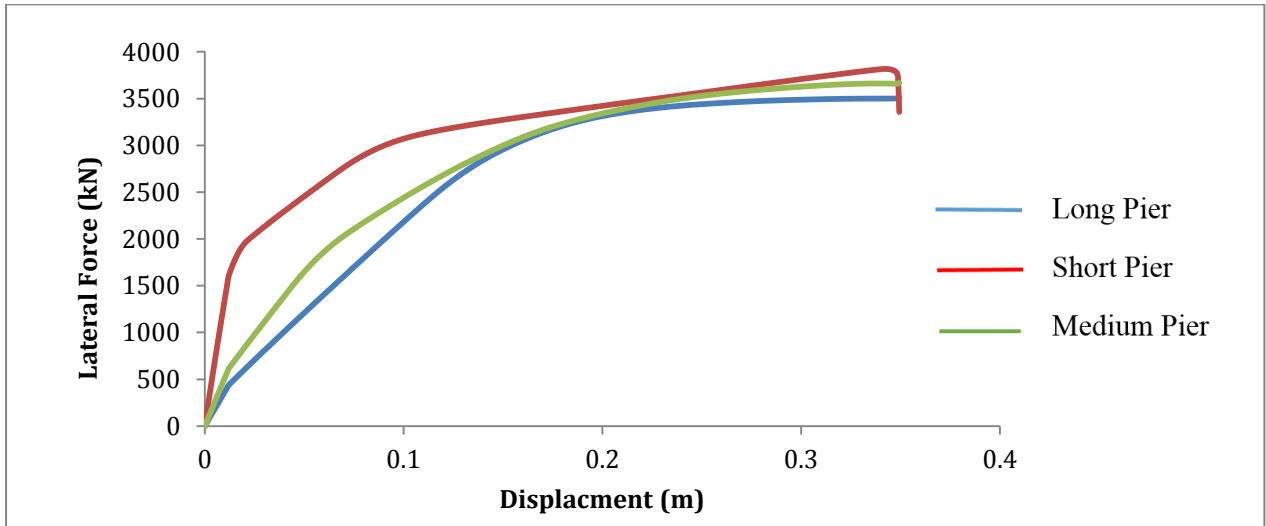


Fig. 20: Shear-displacement curve showing synchronised failure of pier with 16 and 6 metre heights from second scenario of the second case study



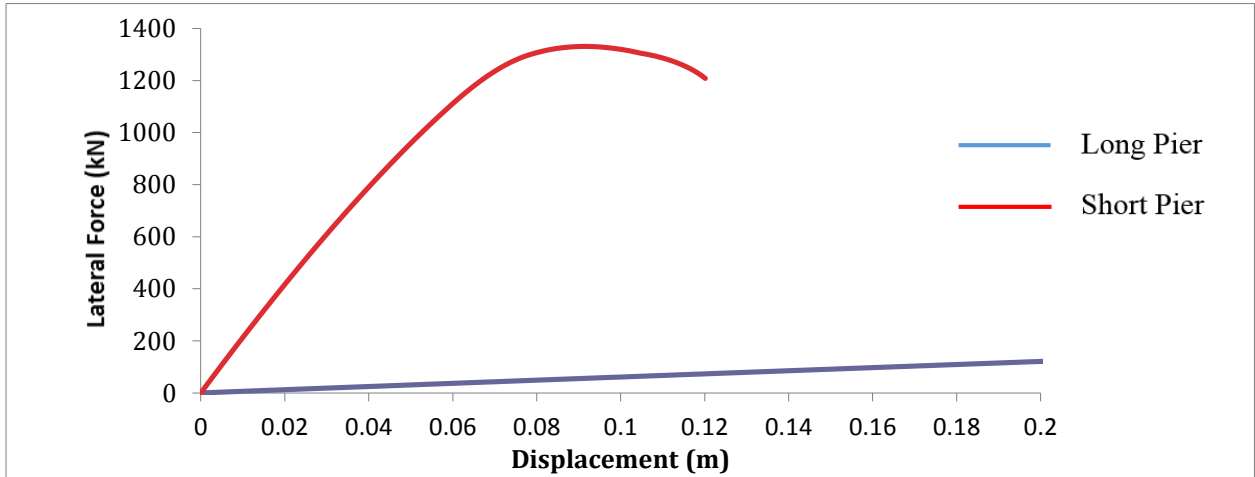


Fig. 21: Shear-displacement curve showing unsynchronised failure of bearing-type bridge with pier height ratio of 0.5

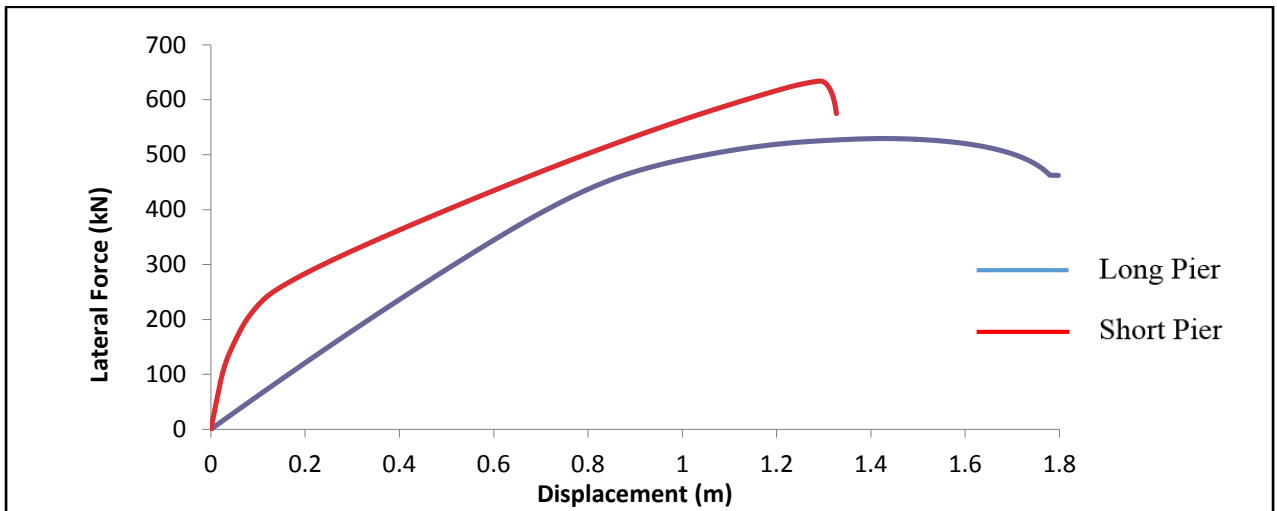


Fig.22: Shear-displacement curve showing synchronised failure of bearing-type bridge with pier height ratio of 0.5

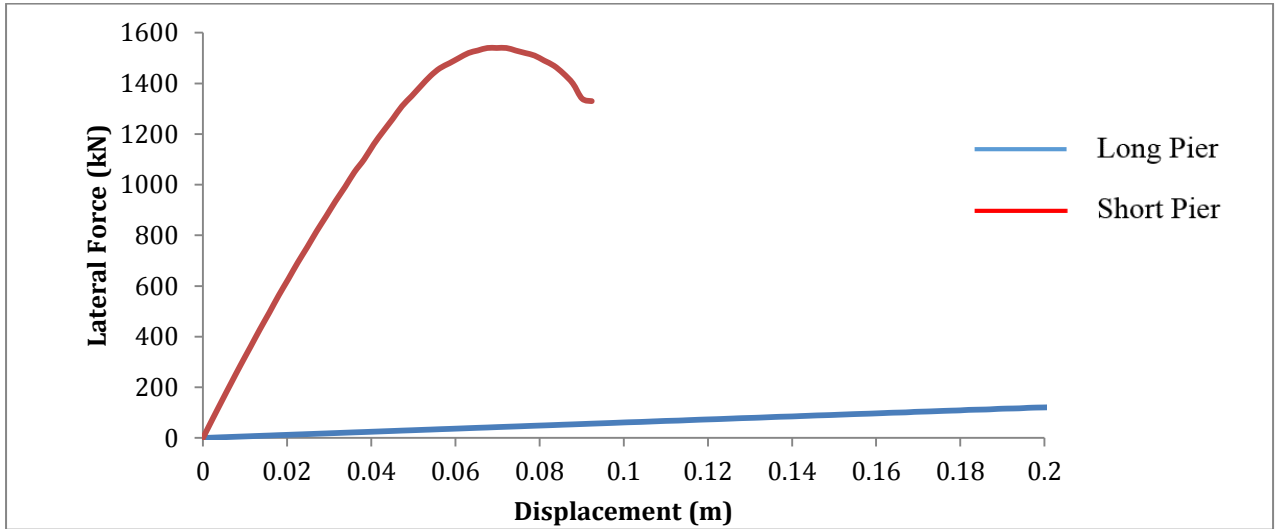


Fig.23: Shear-displacement curve showing unsynchronised failure of bearing-type bridge with pier height ratio of 0.3

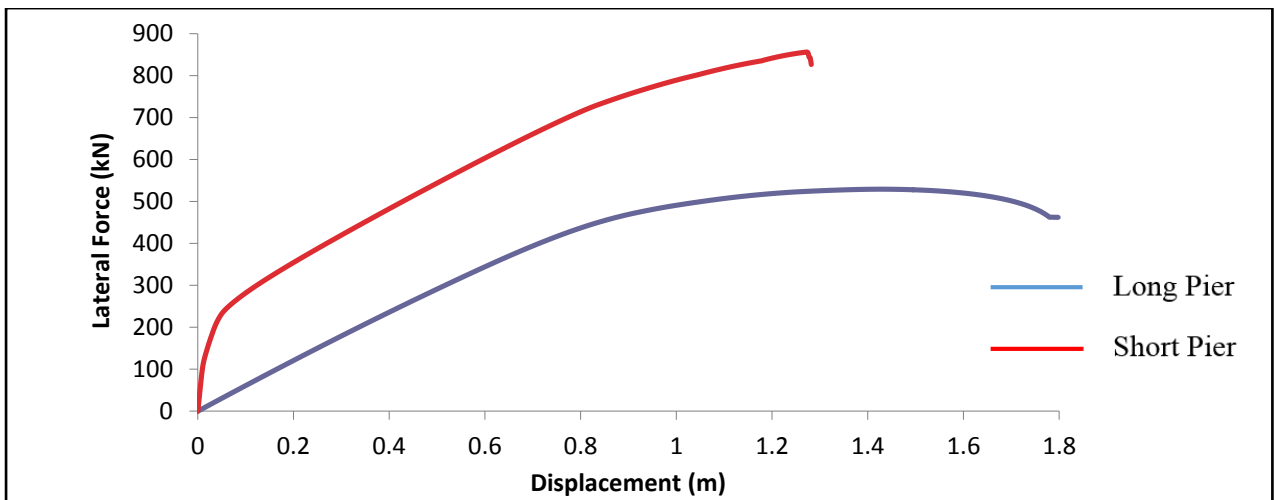


Fig.24: Shear-displacement curve showing synchronised failure of bearing-type bridge with pier height ratio of 0.3

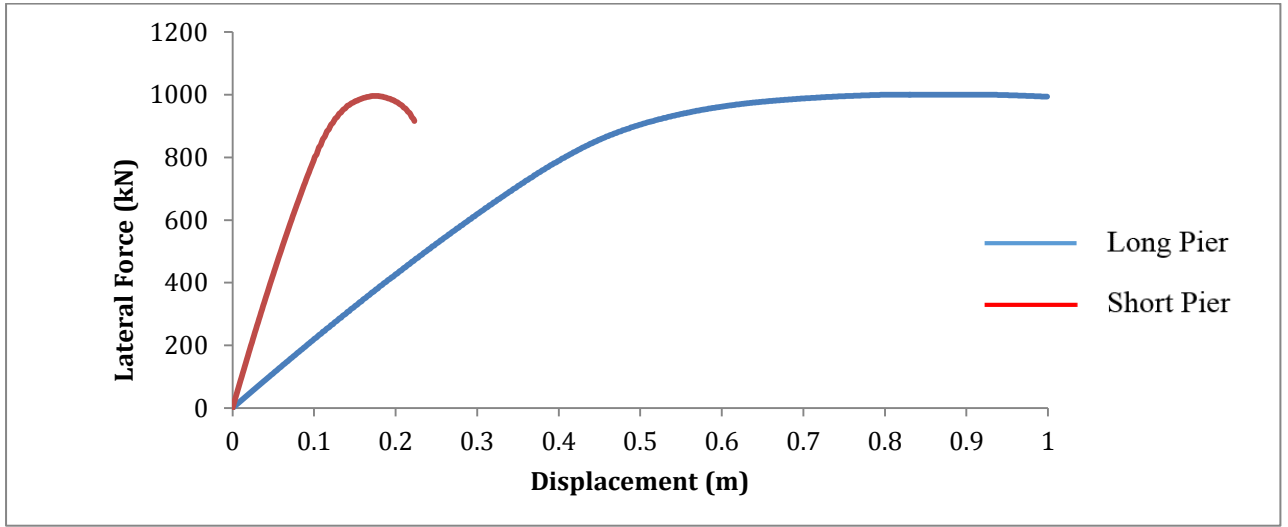


Fig.25: Shear-displacement curve showing unsynchronised failure of combined bridge with pier height ratio of 0.5

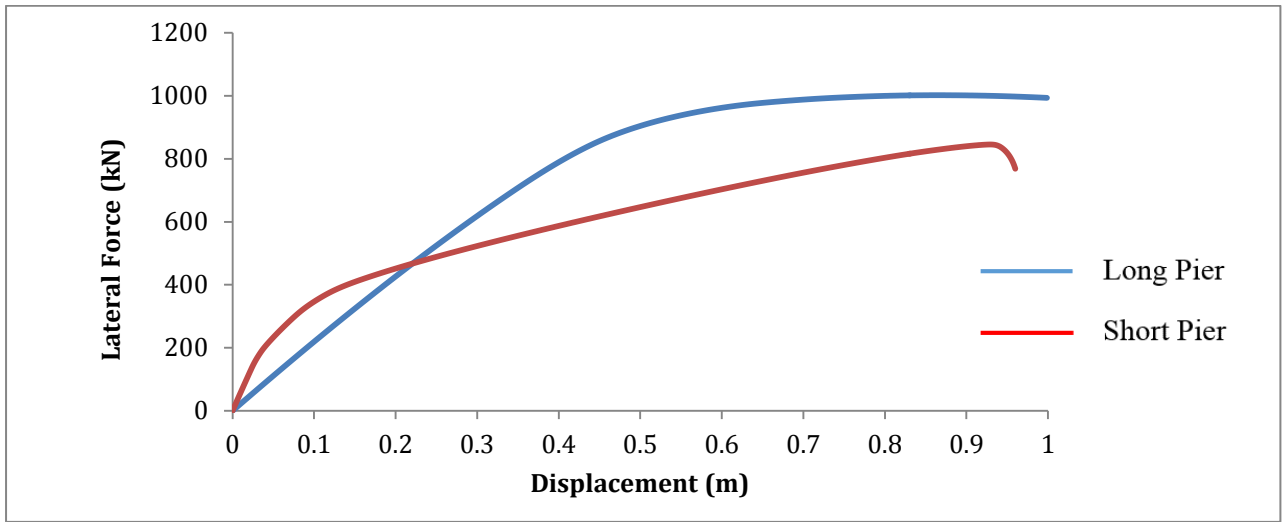


Fig.26: Shear-displacement curve showing synchronised failure of combined bridge with pier height ratio of 0.5

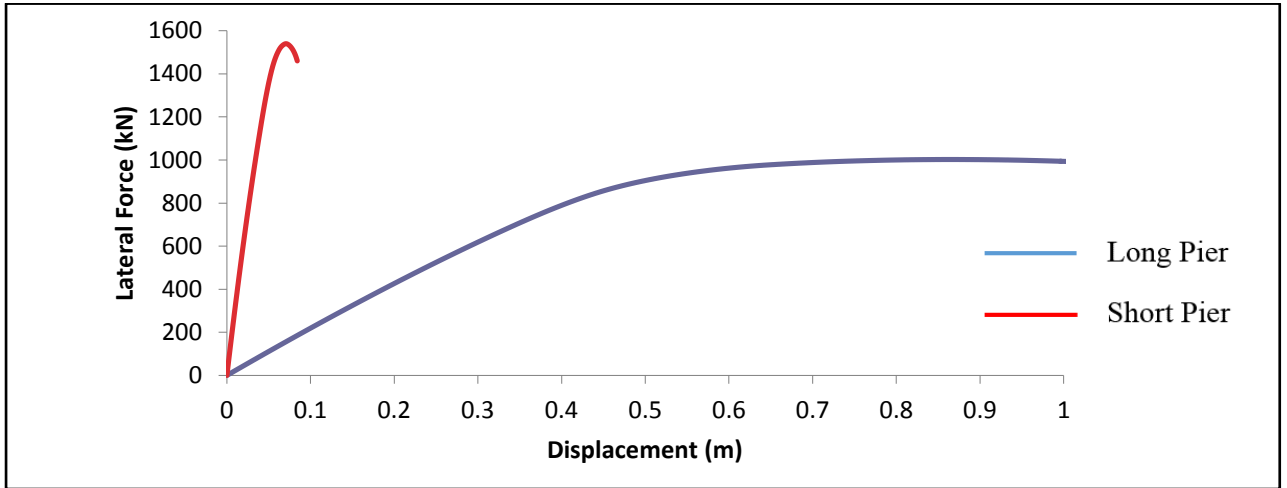


Fig.27: Shear-displacement curve showing unsynchronised failure of combined bridge with pier height ratio of 0.3

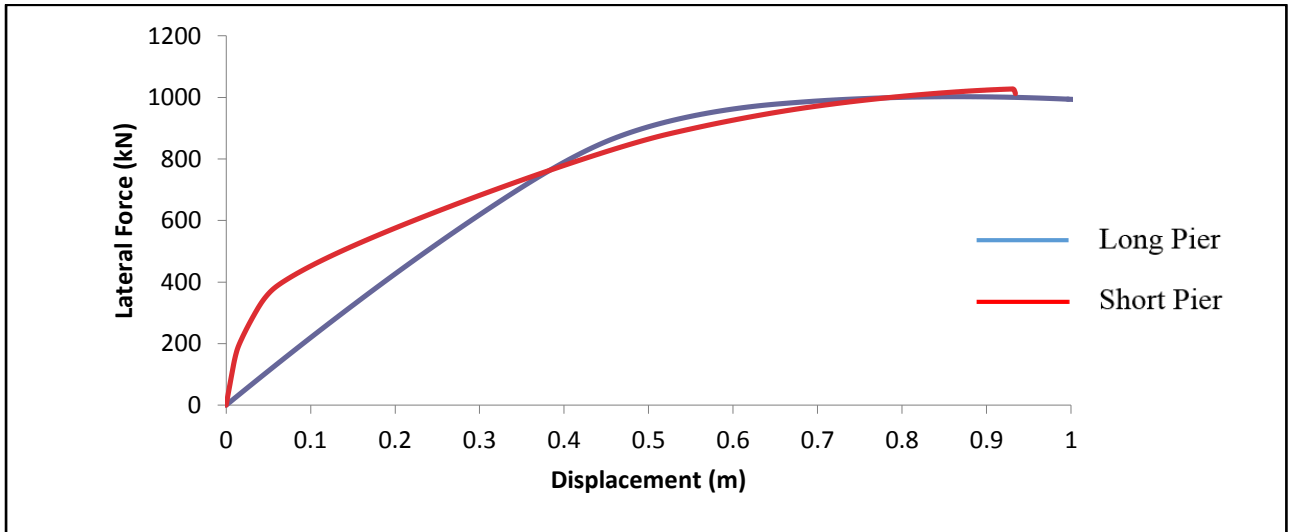


Fig.28: Shear-displacement curve showing synchronised failure of combined bridge with pier height ratio of 0.3

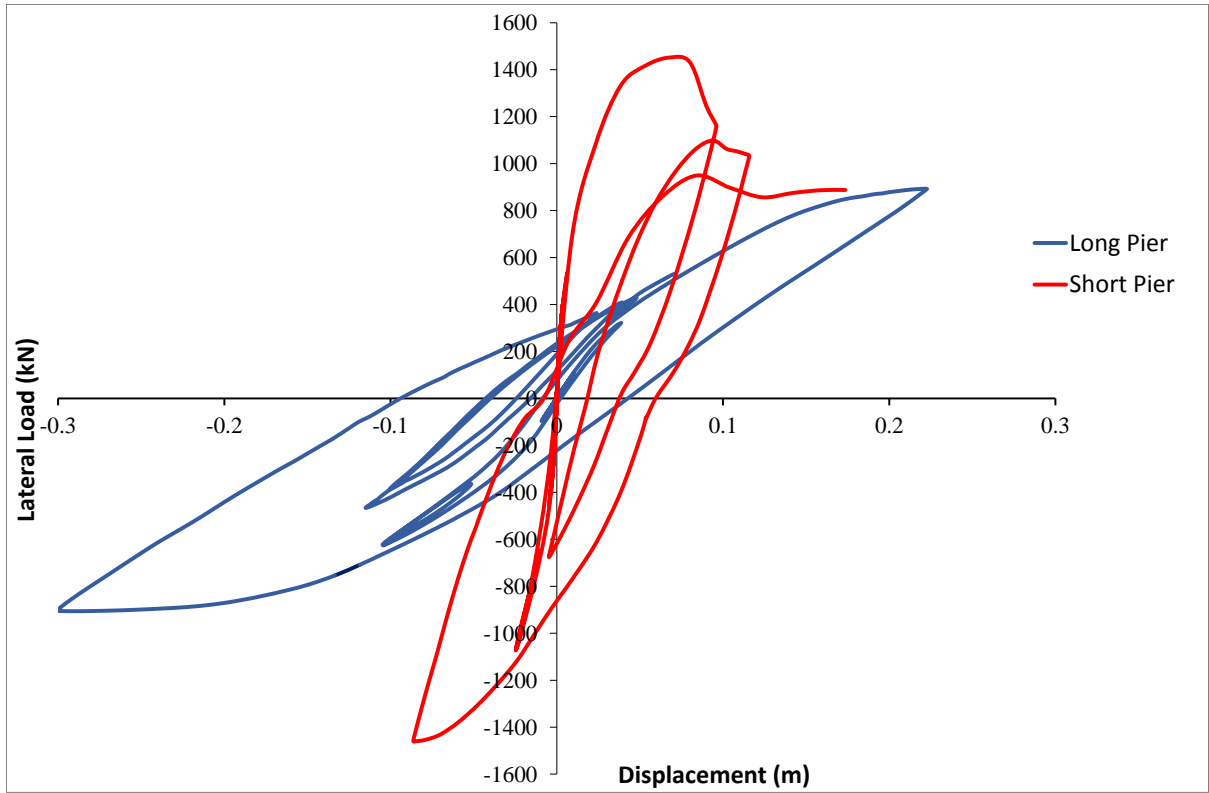


Fig. 29: Dynamic shear-displacement curve showing unsynchronised failure of bridge with pier height ratio of 0.5

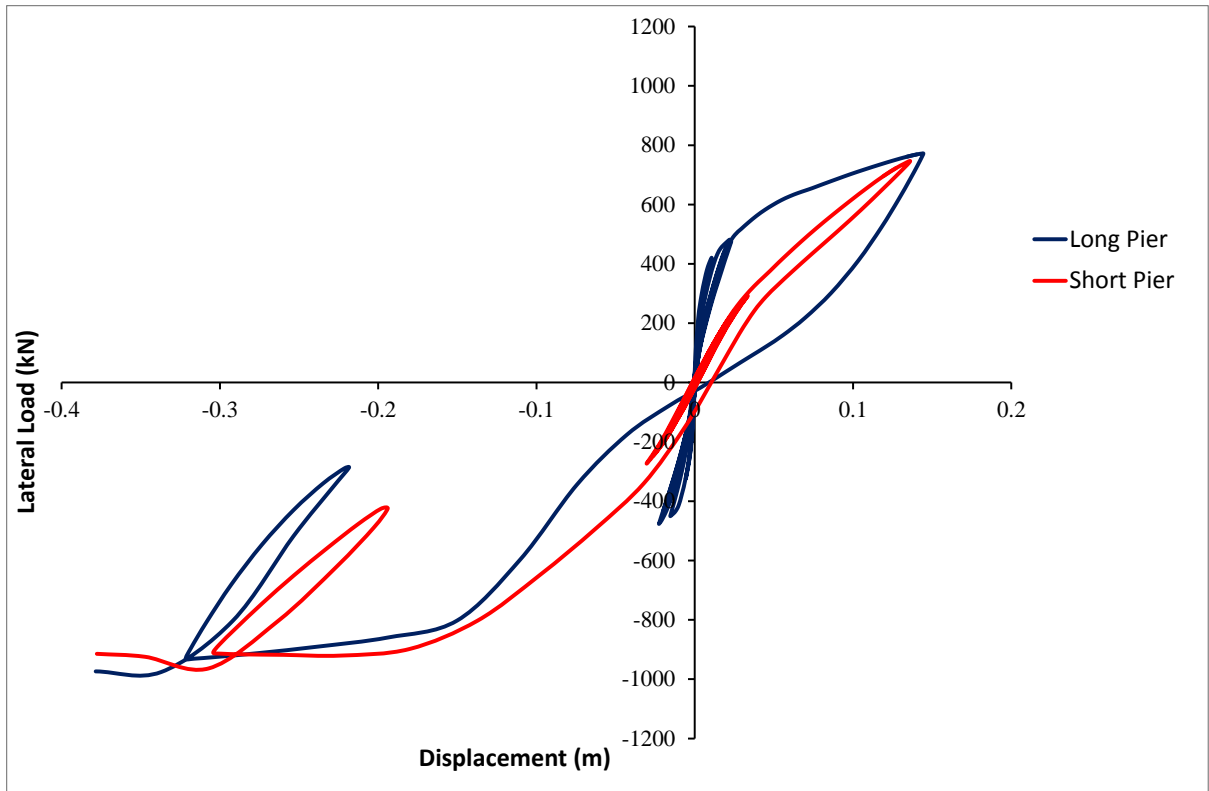


Fig. 30: Dynamic shear-displacement curve showing synchronised failure of bridge with pier height ratio of 0.5

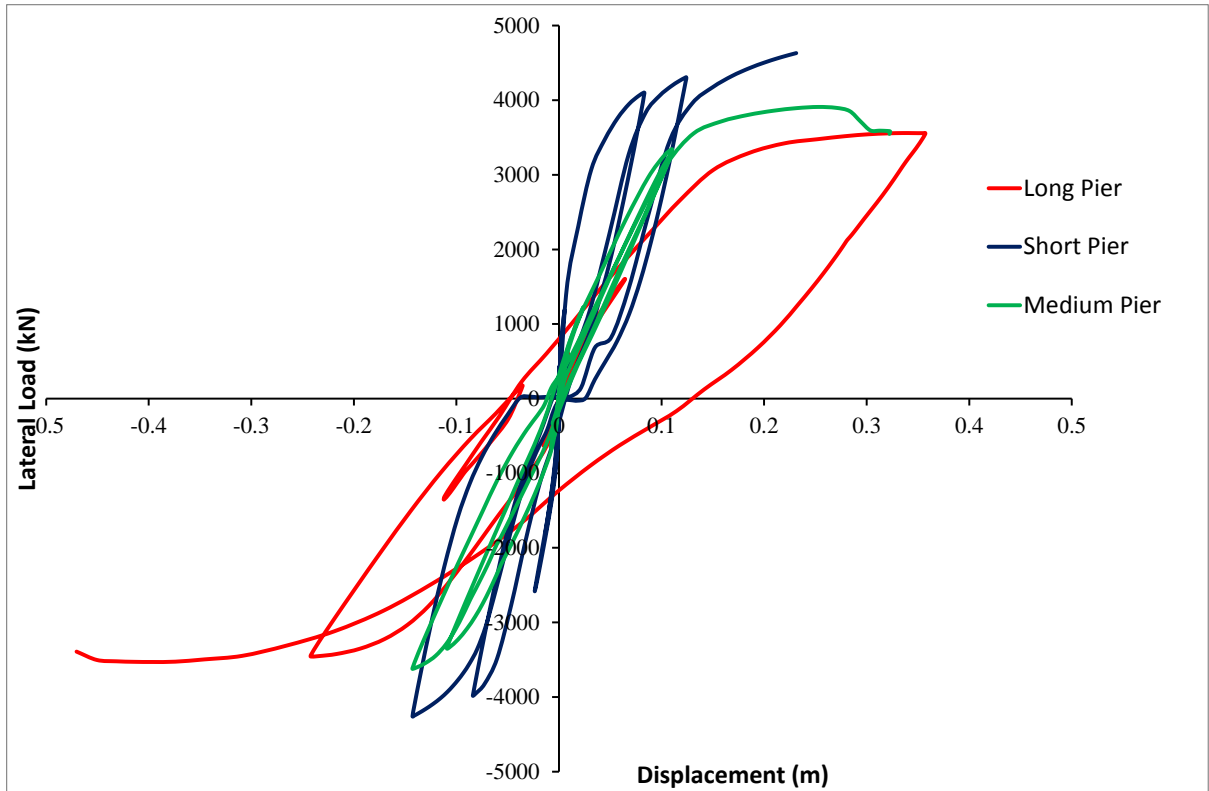


Fig.31: Dynamic shear-displacement curve showing unsynchronised failure of bridge with 16, 6 and 12 metre pier heights

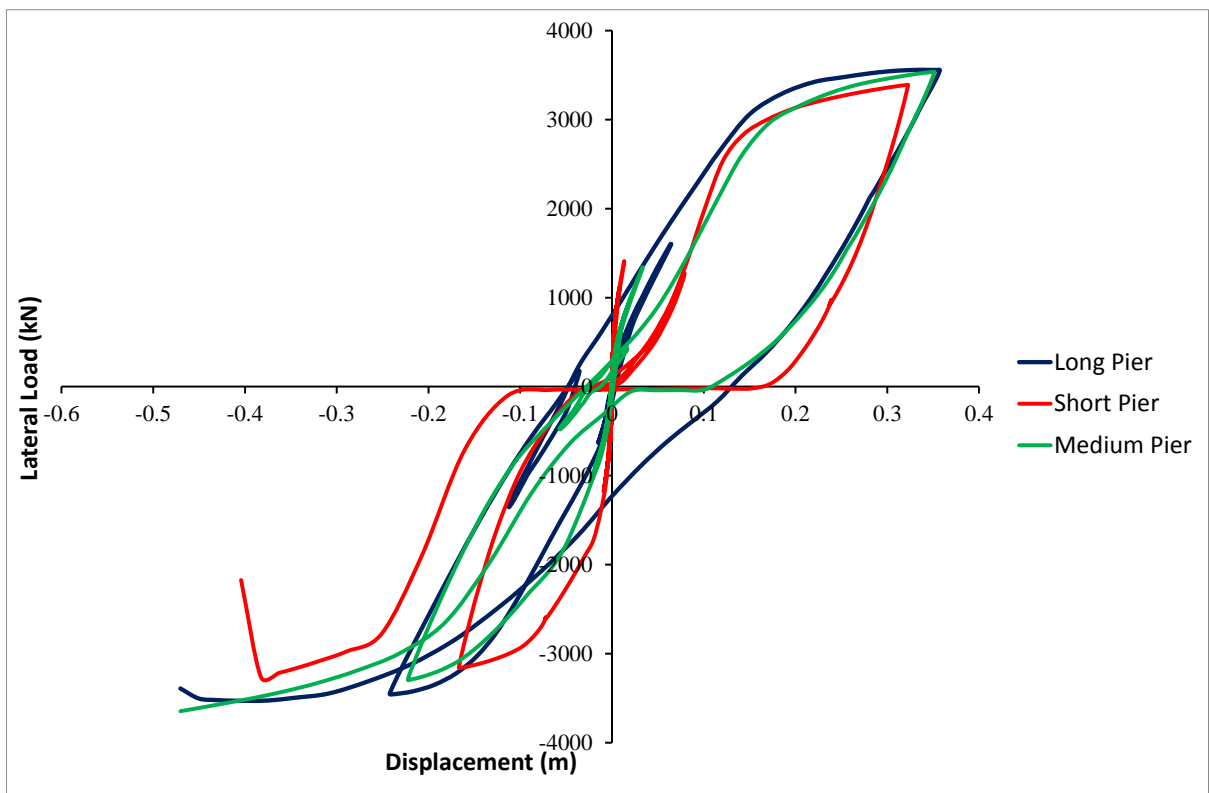


Fig. 32: Dynamic shear-displacement curve showing synchronised failure of pier with 16 and 6 metre heights from second scenario of the second case study

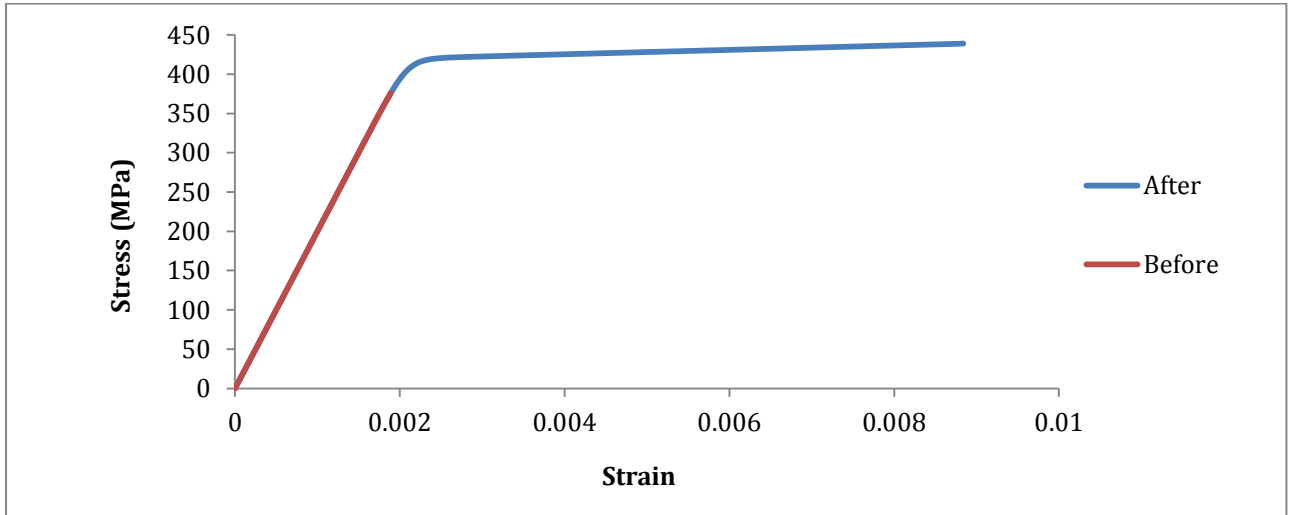


Fig. 33: Stress/strain curve at the pier peak strength for the transverse bars used in 6m pier, before and after regularisation

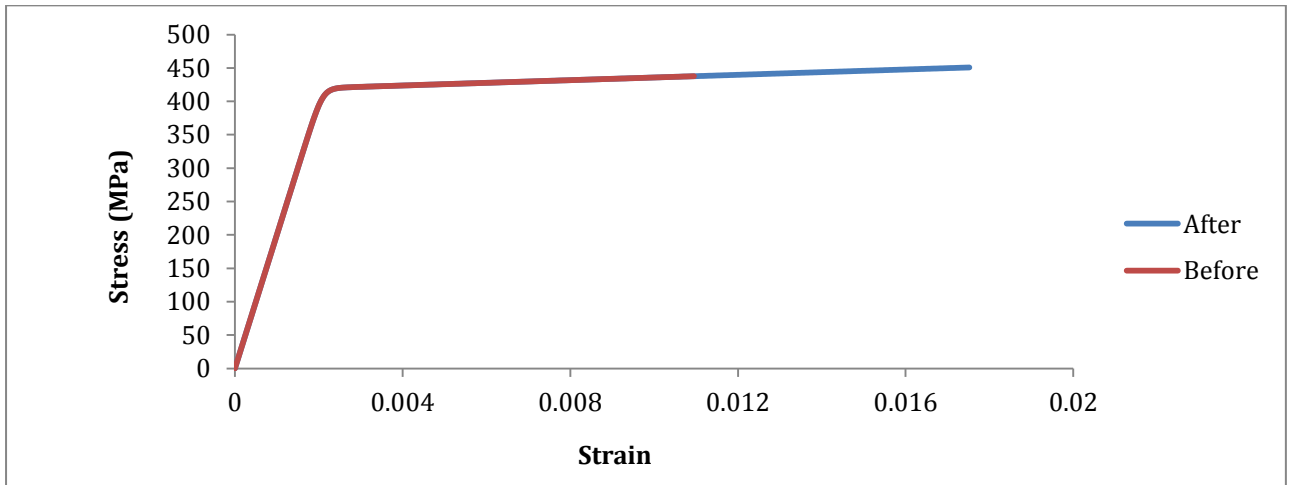


Fig. 34: Stress/strain curve at the pier peak strength for the longitudinal bars used in 6m pier, before and after regularisation